Composite nonlinear feedback control of a DC-DC boost converter under input voltage and load variation

Vazani, Ali; Mirshekali, Hamid; Mijatovic, Nenad; Ghaffari, Valiollah; Dashti, Rahman; Shaker, Hamid Reza; Mardani, Mohammad Mehdi; Dragičević, Tomislav

Published in:
International Journal of Electrical Power and Energy Systems

Link to article, DOI:
10.1016/j.ijepes.2023.109562

Publication date:
2023

Document Version
Publisher's PDF, also known as Version of record

Electrical Power and Energy Systems 155 (2024) 109562

Contents lists available at ScienceDirect

International Journal of Electrical Power and Energy Systems

journal homepage: www.elsevier.com/locate/ijepes

Composite nonlinear feedback control of a DC-DC boost converter under input voltage and load variation

Ali Vazani [a], Hamid Mirshekali [b], Nenad Mijatovic [c], Valiollah Ghaffari [a], Rahman Dashti [d], Hamid Reza Shaker [b,*], Mohammad Mehdi Mardani [c,1], Tomislav Dragičević [c]

[a] Department of Electrical Engineering, Faculty of Intelligent Systems Engineering and Data Science, Persian Gulf University, Bushehr, Iran
[b] SDU Center for Energy Informatics, University of Southern Denmark, Odense DK-5230, Denmark
[c] Department of Wind Energy, Center for Electric Power and Energy, Technical University of Denmark, 2800 Kongens Lyngby, Denmark
[d] Clinical-Laboratory Center of Power System & Protection, Faculty of Intelligent Systems Engineering and Data Science, Persian Gulf University, Bushehr 7516913817, Iran

ARTICLE INFO

Keywords:
Composite Nonlinear Feedback
Boost Converter
Model Predictive Control
Input Voltage Variation

ABSTRACT

Voltage boost converters are one of the most important components of DC microgrids, since they are used to enhance the voltage of naturally intermittent energy sources such as solar panels in order to feed unknown demands. In this work, a novel tuning algorithm for Composite Nonlinear Feedback (CNF) is studied in depth to improve transient performance and address output voltage regulation for a DC-DC boost converter in the presence of DC input uncertainty. The proposed CNF controller comprises both linear and nonlinear feedback terms. The linear part contributes to the stability and output tracking with a small damping ratio and a quick response. The nonlinear part, i.e., damping term, reduces the overshoot stemming from the linear feedback law and increases the damping ratio of the overall closed-loop system. The nonlinear part is automatically tuned whereby the transient performance of the DC-DC boost converter improves significantly. To assess the performance of the proposed technique, a boost converter is simulated in MATLAB Simulink considering different scenarios such as changing load, DC input, and voltage reference. The numerical results demonstrate that the tuned CNF controller outperforms the linear controller in the DC boost converter. Additionally, several experiments are conducted to validate the efficacy of the suggested technique.

1. Introduction

Energy consumption has increased significantly in recent decades, leading to the use of energy production potentials. [1]. Electrical power may be generated by transforming non-conventional renewable energy sources such as wind and solar into grid-compatible forms. Electronic power converters may be employed in a broad range of voltage control applications via the utilization of microgrids [2]. Therefore, one of the most important regulation functions may be found in DC microgrids, especially DC-DC boost converters. The underlying aim is to generate a steady load voltage, albeit with input voltage perturbation and load shift [3]. It is critical to employ an appropriate control strategy in order to address this subject.

The previous works related to the control of boost converters are discussed briefly, as follows. A mixture of conventional proportional-integral-derivative (PID) controllers has been used in numerous investigations. For example, A cascade control strategy was presented to address voltage regulation. To achieve the goal, a dual loop control method was devised, including model predictive control (MPC) in the inner loop and a proportional-integral (PI) controller in the outer loop [4]. Also, the reference governor concept has been applied to PID-precompensated DC boost converters. Intending to improve performance, the MPC approach optimizes such a control strategy. A current observer has also been developed to acquire knowledge about state variables [5]. Similarly, with a dual-loop hybrid DC-DC boost converter, efforts have been made to modify the sliding mode control technique based on classical PI controllers [6]. Besides, an active capacitor voltage balancing control method has been fully introduced for a boost

* Corresponding author.
E-mail addresses: ali.vazani@mehr.pgu.ac.ir (A. Vazani), hmir@mmmi.sdu.dk (H. Mirshekali), nm@dtu.dk (N. Mijatovic), vghaffari@pgu.ac.ir (V. Ghaffari), R.Dashti@pgu.ac.ir (R. Dashti), hrsh@mmmi.sdu.dk (H.R. Shaker), mmema@dtu.dk (M.M. Mardani), tomdr@dtu.dk (T. Dragičević).
[1] M. M. Mardani is also with the Siano-Danish College (SDC), Universitiy of Chinese Academy of Science, Beijing 101408, China.

https://doi.org/10.1016/j.ijepes.2023.109562
Received 5 September 2022; Received in revised form 31 May 2023; Accepted 7 October 2023
Available online 14 October 2023

converter based on the average-behavior circuit model. Furthermore, a proportional (P) and a PI controller have been designed for voltage balancing control loop and output voltage regulation [7]. In the presence of uncertainty and external disturbances, to stabilize a non-minimum phase DC-DC boost converter, a robust PID controller was designed utilizing quantitative feedback theory (QFT) [8]. Parameters adjustment and sensitivity are two of the most challenging aspects of classical PID controllers.

In [9], a nonlinear tracking approach, i.e., energy-shaping with a self-tuner mechanism and disturbance observer (DOB), was used to provide the control law for a DC-DC boost converter. The primary drawback of this study is that it designs the controller without considering the effect of input saturation on the system. In [10], a Min-Type control strategy for a synchronous boost converter based on a nonlinear switching surface was investigated using sliding mode. Furthermore, another dual-loop control strategy based on flatness control has been applied to output series interleaved boost converter integrated into a fuel cell. In addition, a state observer is coupled with such a method to tackle input voltage uncertainty. The inner loop and the outer loop were devoted to current tracking and output voltage regulation respectively [11]. In [12], three-phase interleaved boost converters have undergone the decoupled master–slave current balancing control theory extended to interleave N-phase DC-DC converters. Moreover, for a Floating Interleaved Boost Converter (FIBC) combined with a fuel cell, a dual-loop control mechanism was proposed to yield a constant output voltage. The inner loop controller is based on a super-twisting sliding mode algorithm and the outer loop employs active disturbance rejection control (ADRC) [13]. In the presence of unknown disturbance and model uncertainty, a composite technique comprising MPC and DOB has been applied to the DC boost converter to enhance the steady-state error. The MPC yields appropriate tracking performance, while the DOB eliminates steady-state error [14]. By minimizing a criterion function, the MPC theory has been used to control switching in boost converters. A sliding mode observer has been devised to estimate unknown variables in order to implement such an approach [15]. In addition, pole placement in the desired location [16] and a combination of Kalman filter and MPC [17] have been investigated for controlling DC-DC/AC and DC-DC, respectively. In [18], the Hamiltonian function was used to study the control of a multi-phase interleaved boost converter supplied by a fuel cell.

Moreover, the well-known Linear Quadratic Regulator (LQR) has been studied in many investigations. For instance, Dorin O. *Et al.* [19] have used the loss equation as the performance index for a boost converter to enhance the LQR. One of the main drawbacks of LQR-based methods is that they are not designed robustly against parameter variations and input saturation. Likewise, several control strategies were applied to a boost converter coupled with a fuel cell. For example, Average Current Mode Control (ACMC), LQR, and two modifications of LQR based on the PI controller have been designed to reduce the effect of the series resistance of the output capacitor [20]. A robust LQR based on Linear Matrix Inequality (LMI) minimization technique [21] has been proposed, as well as an extension of LQR to parallel-connected DC-DC boost converters [22]. Similarly, for interleaved DC-DC boost converters integrated into a fuel cell, a combination of two traditional approaches has been thoroughly investigated. On the one hand, for output regulation, the LQR technique was used. On the other hand, the well-known genetic algorithm (GA) has been applied to the LQR controller to optimize the weight matrices in order to achieve better performance [23]. Despite its popularity, the LQR is a traditional approach. Additionally, the GA optimization approach has some restrictions such as being computationally intensive and requiring offline operations. In contrast to conventional CNF methods, a new online passive-based approach has been applied to the CNF controller merely for nonlinear systems [24].

A unique composite nonlinear controller for boost converters is developed in [25]. This work's primary objective is to add a stabilizer under a demanding persistent power load. A nonlinear disturbance observer is included in a backstepping manner to estimate the load fluctuation with a quick and precise dynamic response, taking into consideration the converter's nonlinearity. This work responds adequately even under conditions of heavy loading. This method's dependence on the converter parameters might be listed as one of its drawbacks. For the islanded multi-bus DC microgrids, [26] applies a uniform nonsmoothed control technique. This method ensures large signal stabilization of the microgrid. Towards the practical implementation, the complex line impedance is taken into account. The power-sharing level of the control architecture is done using a decentralized approach. Weighted homogeneity matrices have been used to accomplish this. In this study, a nonsmoothed high gain observer is designed for external disturbances from other grid zones, however, it does not take the system uncertainties into consideration. In the presence of input voltage and parameter change, it may adversely influence the robustness of this methodology. A mixed MPC-sliding mode controller for a hybrid energy storage system is proposed in [27]. A sliding mode observer is created as compensation for the disturbances, however, because of its nonlinear character, it may have a negative impact on the system's stability under unpredictable circumstances. The primary drawback of this technique is that the controller parameters are fixed and incapable of being adjusted in response to an unexpected change in the system. An open-loop control scheme has been proposed by implementing a unity power factor strategy to enhance the performance of boost rectifiers when dealing with low conversion rates in discontinuous conduction mode (DCM). While having the virtue of constant switching frequency, it can be considerably intricate in nature [28]. In [29], A small-signal model of DC-DC PWM converters operating in DCM has been introduced and applied to a buck-boost converter. Nevertheless, a significant limitation of this linear control scheme is its inability to support nonlinearity. Besides, such a control technique has been designed for the ideal converter switching-cell working in both continuous and discontinuous conduction mode [30]. In addition, A systematic synthesis of hybrid feedforward control strategies was developed using the open-loop characteristics of PWM switching converters [31]. The final and crucial point to note in power converter control is that conventional feedback loop designs in DC-DC switch mode systems, previously utilized, rely on frequency domain analysis after linearization around the operational point. The main concern arises when faced with a Right Half Plane Zero, which significantly limits the bandwidth of the closed-loop system [32].

The CNF controller consists of a nonlinear and a linear term. At first, the linear feedback law is designed and then used to construct the nonlinear feedback law. The linear component is utilized to create a closed-loop system with a low damping ratio and fast response. However, the linear feedback law provides a significant overshoot while remaining within the actuator's limits. The nonlinear feedback law has been designed in such a manner that it eliminates overshoot stemming from the linear control law by increasing the overall closed-loop damping ratio.

In this study, a composite nonlinear strategy is proposed to control a DC-DC boost converter supplied by an uncertain DC input; and not solely to generate a constant output voltage, but also to remove the large overshoot. The DC boost converter model is preliminarily presented and then, the CNF control theory is employed intending to achieve such an objective. Initially, the linear control law is optimally designed taking into account the polytypic uncertainty as well as input saturation, resulting in a small control feedback gain. The feedback has a low value since it is meant to provide a control force that is bounded between 0 and 1, leading to substantial overshoots. The nonlinear portion is tasked with the duty of improving transient performance for such systems. As a result, the damping term is calculated in the second step to overcome such difficulty. To enhance the transient performance, a novel tuning algorithm is proposed. Then, the CNF controller is applied to the DC boost converter connected to an uncertain DC input and implemented in MATLAB/Simulink under different scenarios. For further evaluation, a practical test is also performed. The main novelties of this paper are as follows:

- The CNF approach is used on the boost converter.
- The MPC technique is used as a linear component that takes into account system uncertainty and input saturation in the designing procedure.
- A new CNF parameter tuning approach is proposed that automatically updates the regulating parameters to decrease output overshoot.
- The input saturation is taken into account by the online CNF parameters optimizer throughout the tuning process.

In Table 1 the characteristics of this method are compared with two algorithms of generalized predictive control (GPC) and finite set model predictive control (FS-MPC).

The organization of this paper is as follows. In Section 2, the DC-DC boost converter model is described. In addition, the CNF control theory is developed in Section 3. Moreover, simulation, quantitative and illustrative outcomes are reported in Section 4. The experimental verification is presented in Section 5. Finally, in Section 6, noteworthy consequences are summarized.

Table 1
Comparison between the proposed method and GPC and FS-MPC algorithms.

	GPC [34]	FS-MPC [35]	The proposed method
Complexity	Simple	Complex	Complex
Nonlinearity	Linear	Nonlinear	Hybrid
Computational burden	Low	High	Normal
Uncertainties	CS	CS	support
Adaptive	No	No	Yes
Switching frequency	Constant	Variable	Constant
Stability analysis	Yes	No	Yes
Robustness	No	No	Yes

CS: Cannot support

2. Converter model

The DC-DC boost converter's architecture is shown in Fig. 1. This converter has a direct current input that receives power from DC sources such as solar panels, and fuel cells. Three main elements of an inductor, a diode, and a power switch are used to increase the input voltage in this system. A capacitor is connected to the boost converter's output, which helps to stabilize and minimize the ripples in the output voltage. Finally, a load in form of controllable resistors is connected to an output capacitor.

The following is a short description of the converter modeling:

$$L.\frac{dI_L}{dt} = V_{DC} - V_o(1-d) \tag{1}$$

$$C.\frac{dV_o}{dt} = I_L(1-d) - \frac{V_o}{R} \tag{2}$$

where V_{DC} is the input voltage, V_o is the output of the converter which is also the voltage of the capacitor, L and C are the inductance and capacitors, respectively. d is the duty cycle of the power switch, R_1 and R_2 are the resistive loads connected to the converter's output. The model needs to be linearized around the equilibrium point. Besides, to eliminate the steady-state error of output voltage under load shift and input voltage uncertainties an integral part is augmented to the state space model. The required quantities are determined by two measurements of inductor current and capacitor voltage. The state-space equation of the boost converter is as follows:

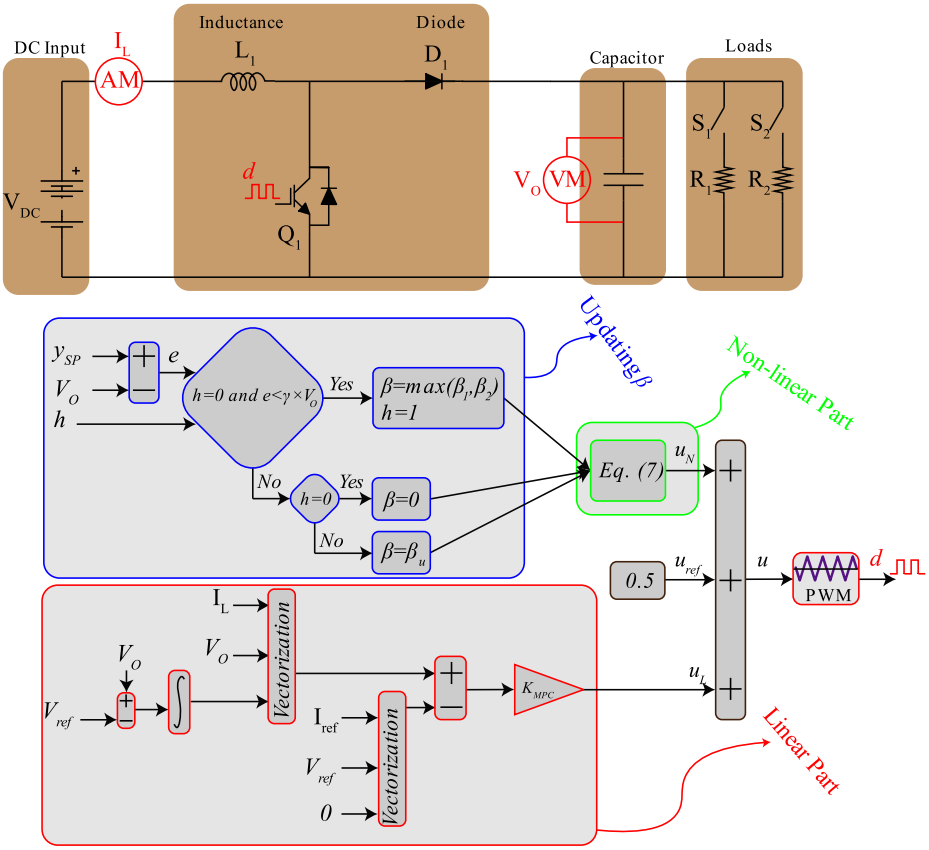

Fig. 1. Topology and control scheme of the DC-DC boost converter.

$$\begin{bmatrix} \dot{x}_1 \\ \dot{x}_2 \\ \dot{x}_3 \end{bmatrix} = \begin{bmatrix} 0 & \frac{(1-d_n)}{L} & 0 \\ \frac{(1-d_n)}{C} & -\frac{1}{RCd_n^2} & 0 \\ 0 & -1 & 0 \end{bmatrix} \cdot \begin{bmatrix} x_1 \\ x_2 \\ x_3 \end{bmatrix} + \begin{bmatrix} \frac{V_{DC}}{Ld_n} \\ -\frac{V_{DC}}{RCd_n^2} \\ 0 \end{bmatrix} d \tag{3}$$

where x_1 and x_2 are the difference between the inductor current and capacitor voltage with their reference values and x_3 is the integral of output voltage. The equilibrium point of control input is chosen to be $d_n = 0.5$. Reference vector is $X_{ref} = [I_{ref}, V_{ref}, 0]^T$. In this model, the control output of the PWM generator is bounded between 0 and 1 for sufficient operation because of the natural saturation of PWM. It is noteworthy that rapid changes in the control input cause the inductor current to fluctuate. By considering polytopic uncertainty for the converter the system's model and LMI problem can be rewritten. The converter model consists of inductor (L), capacitor (C), input voltage (V_{in}), and a resistor (R) as its load that can be uncertain. By considering these parameters between a lower and an upper bound as follows:

$$L_{min} < L < L_{max}$$

$$V_{inmin} < V_{in} < V_{inmax}$$

$$C_{min} < C < C_{max}$$

$$R_{min} < R < R_{max}$$

We have:

$$\dot{x} = Ax + Bsat(u)$$

where A and B consist of uncertain parameters. There are four parameters with two adverse conditions each. There are 16 possible combinations of uncertainties for the state space system. Therefore, we have the state space system as follows:

$$\dot{x} = A_i x + B_i sat(u) \quad i \in \{1, 2, \cdots, 16\}$$

3. The proposed approach

3.1. Composite nonlinear feedback control theory

Consider the following nominal linear saturated system:

$$\begin{cases} \dot{x} = Ax + Bsat(u) \\ y = Cx \end{cases} \tag{4}$$

where x is the state vector, u is the constrained control input and y is the measured output. Besides, A, B and C are constant matrices. Moreover, the actuator saturation is defined as:

$$sat(u) = \begin{cases} u_{max} & u > u_{max} \\ u & u_{min} \le u \le u_{max} \\ u_{min} & u < u_{min} \end{cases} \tag{5}$$

where u_{max} and u_{min} are the saturation levels of input. The CNF controller is constructed based on the assumption of stabilizability, detectability, and invertibility of system matrices. The CNF controller will be set up such that the output tracks a reference signal y_r quickly and without large overshoot or adverse effects of actuator saturation. The composite nonlinear feedback control law is established assuming that all states of a given system described by (4) are measurable.

The nonlinear system's equilibrium points in Eq. (4) are calculated as follows. The control signal $\bar{u}$ propels the output to track a constant reference:

$$\begin{cases} A\bar{x} + B\bar{u} = 0 \\ C\bar{x} = y_r \end{cases} \tag{6}$$

Take note that with a boost converter, the output voltage is constant but the inductor current varies with the load. The inductor current is considered constant and determined using nominal values for simplicity. However, a disturbance observer may be constructed to continuously update the inductor current. The linear control feedback should be designed as follows:

$$u_\lambda = \Pi x + \tau \tag{7}$$

where τ is a scalar term computed later in (8) and Π is a gain matrix of u_λ. The gain matrix Π can be derived employing LQR, LQG, LQ, H_2 or solving LMI-based minimization problem (providing that $A + B\Pi$ is an asymptotically stable matrix, and the closed-loop system has a small damping ratio and quick response). Likewise, such a feedback law always maintains within the saturation limits, (i.e., $u_{min} \le u_\lambda \le u_{max}$). Take such a definition $\xi \triangleq x - \bar{x}$ into consideration. The steady-state value of u_L is expressed as

$$\bar{u} = \Pi\bar{x} + \tau \tag{8}$$

By substituting Eq. (8) into Eq. (7) the linear part of the CNF controller can be modified as follows:

$$u_\lambda = \bar{u} + \Pi\xi \tag{9}$$

The nonlinear feedback law is considered as follows:

$$u_\nu = \Omega(y_r, y)B^T\Sigma\xi \tag{10}$$

where $\Omega(y_r, y)$ can be any nonpositive locally Lipschitz function in y and y_r. While the output tracks the reference input, $\Omega(y_r, y)$ is used as a damping term to modify the damping ratio. Σ is also a positive definite matrix that will be obtained to improve the damping ratio of the whole closed-loop system. Finally, the u_{CNF} is defined as follows:

$$u_{CNF} = \Pi\xi + \bar{u} + \Omega(y_r, y)B^T\Sigma\xi \tag{11}$$

3.2. Selection of the nonlinear Function $\Omega(y_r, y)$

As mentioned earlier, nonlinear feedback law is utilized to enhance the damping ratio and minimize the overshoot produced by linear feedback law. The challenge in developing the nonlinear portion u_ν in Eq. (10) is to choose a nonlinear function that will increase the closed-loop system's transient performance as the measured output approaches the reference input. $\Omega(y_r, y)$ is selected as a function of tracking error by defining tracking error $\varepsilon \triangleq y_r - y$. As a consequence, assuming that $\Omega(y_r, y) \le 0$ for all y_r and y, the nonlinear function assures the stability of the closed-loop system. Although Ω selection is not unique, the nonlinear function must be deliberately chosen to have the following properties [24]:

Property 1: At the outset of running the system, when the tracking error is very large, the nonlinear function should be in the vicinity of zero. Therefore, the damping term performs ineffectively.

Property 2: When the system's output approaches the reference signal and is in the locality of the setpoint, the nonlinear function should be at its maximum amplitude. Therefore, the damping term performs immensely more effectively.

The nonlinear function is often selected in exponential form. A scalar nonlinear function proposed in [33] is as follows:

$$\Omega(y_r, y) = -\rho e^{-\alpha_0 \alpha |y_r - y|} \tag{12}$$

where $\alpha > 0$ and $\rho > 0$ are constant tuning parameters. Also, α_0 is a scalar parameter given by:

$$\alpha_0 = \begin{cases} \frac{1}{|y_0 - y_r|} & y_0 \neq y_r \\ 1 & y_0 = y_r \end{cases} \tag{13}$$

The performance of the closed-loop system is significantly more

robust to reference target variation since α_0 varies with various reference input y_r. Because the nonlinear function Ω changes from 0 to ρ as the measured output approaches signal reference, it possesses both of the aforementioned properties. The novel tuning technique will be thoroughly investigated in the next section.

3.3. CNF controller gain tuning

The CNF control design was fully investigated in the previous section. At this point, the CNF controller parameters will be designed and tuned during two phases. Using the following quadratic performance index to design the controller parameters optimally at the beginning of the first phase [24].

$$J = \int_{t_0}^{+\infty} \left[(x-\bar{x})^T Q (x-\bar{x}) + (u_\lambda - \bar{u})^T R (u_\lambda - \bar{u})\right] dt \tag{14}$$

The damping term is removed from Eq. (14). Hence, during the following phase, the nonlinear function Ω will be tuned employing the suggested approach. Furthermore, if such a $u_\theta = \min\{\bar{u} - u_{min}, u_{max} - \bar{u}\}$ meets the criterion $\|u_\lambda - \bar{u}\| \le u_\theta$, the linear part of the CNF controller will maintain within the saturation levels. Thus, the linear and nonlinear control law gain matrices will be obtained by minimizing the performance index provided in Eq (14). An LMI minimization-based approach solves such a problem under some LMIs in an offline way which results in stability. Note that, a parametric polytopic uncertainty as well as input control saturation of the boost converter is taken into consideration.

Theorem: the following minimization problem will be feasible under some LMI constraints if there are some matrixes $X = X^T > 0$, G, and scalar γ such that:

$\min \gamma$

subject to:

$$\begin{bmatrix} u_\theta^2 & G \\ * & X \end{bmatrix} \ge 0 \tag{15}$$

$$\begin{bmatrix} X & \xi(t_0) \\ * & 1 \end{bmatrix} > 0 \tag{16}$$

$$\begin{bmatrix} A_i X + B_i G + X A_i^T + G^T B_i^T & X & G^T \\ * & -\gamma Q^{-1} & 0 \\ * & * & -\gamma R^{-1} \end{bmatrix} < 0, \quad i \in \{1, 2, \cdots, 16\} \tag{17}$$

Then the overall closed-loop system is asymptotically stable with $\Pi = GX^{-1}$ and $P = \gamma X^{-1}$. For damping ratio improvement, the gain matrix of equation (11) can be obtained using $\Sigma = P$.

Proof. The matrix inequality of (17) can be modified as follow by using Schur complement with the assumption of $i = 1$ (then it can be written for all possible 16 states):

$$AX + BG + XA^T + G^T B^T + \frac{1}{\gamma} XQX + \frac{1}{\gamma} G^T R G \le 0 \tag{18}$$

Let multiply the inequality of (18) both on the left and right by $\gamma^{\frac{1}{2}} X^{-1}$. Consider the definitions $\Pi = GX^{-1}$, and $P = \gamma X^{-1}$, then

$$PA + PB\Pi + A^T P + \Pi^T B^T P + Q + \Pi^T R \Pi \le 0 \tag{19}$$

Thus,

$$\xi^T (PA + PB\Pi + A^T P + \Pi^T B^T P)\xi \le -\xi^T (Q + \Pi^T R \Pi)\xi \tag{20}$$

Consider the overall closed-loop system with the CNF control law as follow

$$\begin{cases} \dot{\xi} = (A + B\Pi)\xi + B\omega \\ y = C\xi + y_r \end{cases} \tag{21}$$

$$\omega = sat(u_{CNF}) - u_\lambda$$

Take the well-known Lyapunov function into account as $V(\xi) = \xi^T P \xi$. The time-derivative of the Lyapunov function along the closed-loop system trajectories is specified as:

$$\dot{V}(\xi) = \xi^T (PA + PB\Pi + A^T P + \Pi^T B^T P)\xi + 2\xi^T PB\omega \tag{22}$$

The term $2\xi^T PB\omega$ is always negative since $\omega = sat(u_\lambda + u_\nu) - u_\lambda$ and $u_{min} \le u_\lambda \le u_{max}$. from (20) and (22) we have:

$$\dot{V}(\xi) < -\xi^T (Q + \Pi^T R \Pi)\xi \tag{23}$$

which implies asymptotic stability. Likewise, by using the Schur complement, the inequality of (16) can be rewritten as

$$\xi^T X^{-1} \xi < 1 \tag{24}$$

Let multiply both sides of the inequality of (24) by γ and integrate both sides of the inequality of (23), then

$$\xi^T P \xi < \gamma \tag{25}$$

and

$$V(\xi) = \xi^T P \xi > J \tag{26}$$

Both inequalities (25) and (26) result in

$$J < \gamma \tag{27}$$

Utilizing Schur complement the inequality of (15) can be rewritten as $X - G^T u_\theta^{-2} G \ge 0$. Let pre- and post-multiply by X^{-1}, then

$$\Pi^T \Pi \le u_\theta^2 X^{-1} \tag{28}$$

Consider pre-multiply by ξ^T and post-multiply by ξ, then the inequality of (28) is equivalent to

$$\xi^T \Pi^T \Pi \xi \le u_\theta^2 \xi^T X^{-1} \xi \tag{29}$$

Using the inequality of (24), the inequality of (29) can be rewritten as $(u_\lambda - \bar{u})^T (u_\lambda - \bar{u}) \le u_\theta^2$ results in $\|u_\lambda - \bar{u}\| \le u_\theta$. It completes the proof.

The most important portion of CNF tuning occurs in the second phase when the parameters of the nonlinear function (i.e., α and ρ) characterized in Eq. (12) are tuned. At the start of phase II, consider a zone around the set-point y_r as an error bound and the error can be clearly limited by any value. The error bound turns out to be a coefficient of the reference signal y_r, ($|y_r - y| \le \delta y_r$ where $0 < \delta \le 1$). The maximum point of nonlinear feedback law is determined based on the selected nonlinear function and the following lemma, since u_ν is at its maximum magnitude at the start of adding the nonlinear part and then gradually and smoothly decreases.

Lemma 1. *Let $G(s) = C(sI - A)^{-1}B + D$ be $p \times p$ transfer function matrix where (A, B) is controllable and (A, C) is observable. Then $G(s)$ is strictly positive real if and only if there exist matrices $\Sigma = \Sigma^T > 0$, L, and W and a positive constant η such that.*

$$\Sigma A + A^T \Sigma = -L^T L - \eta \Sigma \tag{30}$$

$$\Sigma B = C^T - L^T W \tag{31}$$

$$W^T W = D + D^T \tag{32}$$

It is simple to determine whether the closed-loop system in Eq. (4) is strictly positive real or not at the operational point using the gain matrix Π. By substituting $B^T \Sigma = C$ into Eq. (10), the nonlinear part of the CNF controller, i.e., u_ν will be simplified as

$$u_\nu = -\Omega(y_r, y)[y_r - y] \tag{33}$$

$$u_\nu = -\varepsilon\Omega(y_r, y) \tag{34}$$

Furthermore, using Eq. (12) and the derivative of u_ν Eq. (34), the maximum point of u_ν will be $|\varepsilon| = 1/\alpha$. Thus, α is determined as $\alpha = 1/\delta y_r$. Indeed, δ specifies the instant as the damping term is applied to the CNF control law. Moreover, to fulfill the needs of the designer, δ may be coordinated with desirable transient performance, such as overshoot and settling time. On the one hand, the lower the δ, the greater the overshoot and quick response. On the other hand, the larger the δ the smaller the overshoot and the slower the response. The parameter ρ will be automatically adjusted at this point. The nonlinear control law is added to the CNF controller when the system output enters the error bound, and the state vector at that moment is denoted by $\hat{x}$. Therefore,

$$u_{CNF}(\hat{x}) = u_{max} \tag{35}$$

$$u_{CNF}(\hat{x}) = u_{min} \tag{36}$$

ρ_1 and ρ_2 solve the equations. (35) and (36), respectively, and then the optimal value of ρ is calculated as follows:

$$\rho = max(\rho_1, \rho_2) \tag{37}$$

3.4. Stability analysis

Fundamentally, an s-plane describes the physical system and provides information about poles, zeros, and locations. According to this data, a myriad number of critical characteristics, for instance, stability status can be discovered. In this study, the eigenvalue domain analysis is also examined in addition to the proof of stability.

By utilizing Eq. (21), if $u_{min} \le \bar{u} + \Pi\xi + u_\nu \le u_{max}$, then

$$\omega = \Omega(y_r, y)B^T\Sigma\xi \tag{38}$$

and, thus

$$\dot{\xi} = (A + B\Pi)\xi + B\Omega(y_r, y)B^T\Sigma\xi \tag{39}$$

Since the boost converter is a nonlinear system, the overall closed-loop system in Eq. (39) is linearized around the equilibrium point, and the eigenvalues are calculated and plotted in Fig. 2. The eigenvalues of the entire closed-loop system via the CNF controller obtained for the optimal $\rho = 9.4300\text{e}-07$ are $[-4.7575,\ -0.0411,\ -0.0086]\text{e}+04$.

As can be seen in Fig. 2, since all the eigenvalues for various values of ρ lie on the left-hand side of the s-plane, this power electronic system is stable. Besides, the eigenvalues are sufficiently far from the instability border (imaginary axis), resulting in a quick response.

To sum up, the stability is not only proved in the previous subsection but also, is conspicuous in the eigenvalue domain analysis. On top of this, the location of the poles implies the desired transient. In addition to these, the following simulations and experimental tests confirm the stability and transient performance improvement.

4. Simulation results

To evaluate the suggested CNF method's performance, a DC-DC boost converter is simulated in MATLAB Simulink environment in this section. The proposed CNF and MPC strategies are evaluated under a range of operating scenarios, including DC input fluctuation, reference voltage step change, and load shift, in order to determine the influence of CNF on the transient performance of a non-optimal linear controller. The simulation parameters that are the same as practical ones are presented in Table 2. In $t = [0, 0.5]$ s the controller is enabled to track $V_{ref} = 50V$ for the sake of compensating inductor current below $60A$. The current spike is unavoidabe as a result of the capacitor inrush current. The reference voltage increases at $t = [0.1, 0.15]$ s with a constant slope

Table 2
Parameters of the converter and simulation.

Parameter	Description	Value
V_{in}	Input Voltage	N = 50 v, max = 60 v, min = 30 v
L	Inductor	N = 0.86 mH, max = 1.075 mH, min = 0.645 mH
C	Capacitor	N = 1.1 mF, max = 1.375 mF, min = 0.825 mF
R	Resistive Load	N = 50 Ω, max = 200 Ω, min = 5 Ω
Π	Feedback Gain	$1e^{-3} \times [-7.9 \quad -2.5 \quad 6.5]$
P	Decision Matrix	$1e^{3} \times \begin{bmatrix} 0.0106 & 0.0032 & -0.0085 \\ 0.0032 & 0.0041 & -0.0052 \\ -0.0085 & -0.0052 & 1.661 \end{bmatrix}$
α	Optimized Scalar	0.99
G	Variable Matrix	$[-31.1641 \quad -1.1973 \quad 0.0021]$
ρ	Scalar	$8.7263 \times e^{-7}$

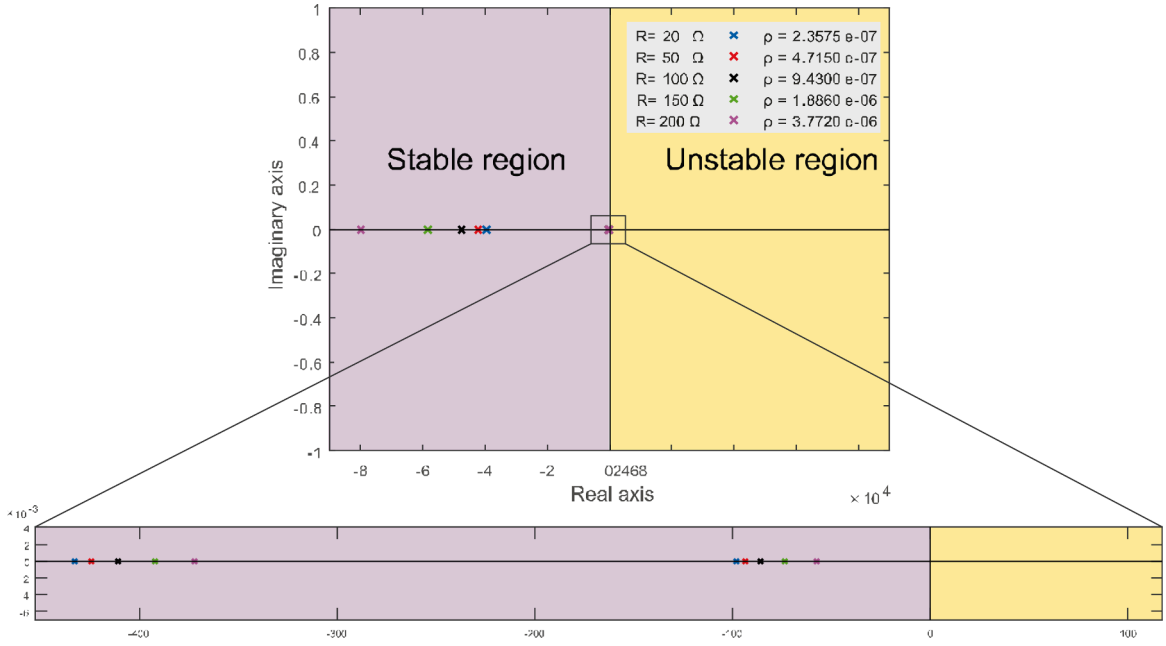

Fig. 2. Eigenvalues of the overall closed-loop power electronic system.

from 50 to 100. The output voltage and current, as well as the inductor current, are shown in Fig. 3 during this transition. As shown, the suggested CNF controller provides quicker response and a reduced overshoot owing to the nonlinear component. Due to the integral component, both controllers have a constant output voltage error of zero.

As shown, the suggested CNF controller provides quicker response and a reduced overshoot owing to the nonlinear component. Due to the integral component, both controllers have a constant output voltage error of zero.

The effect of DC input variation on the controller performance is the second scenario. At 0.3, 0.4, 0.5, and 0.6 s, the input voltage changes from 50 to 60 to 40 to 60 to 50 V. As shown in Fig. 4, the addition of the nonlinear portion to the linear controller results in a substantial improvement in output quantities. For instance, in the case of a step-change in DC input at $t = 0.5$ sec the proposed controller has a much better and softer transition compared to the linear one. The linear controller's voltage overshoot is close to 30%, whereas the CNF controller's voltage overshoot is less than 5%. Take note that while using a linear controller, the inductor current rises to more than 20 A. The third

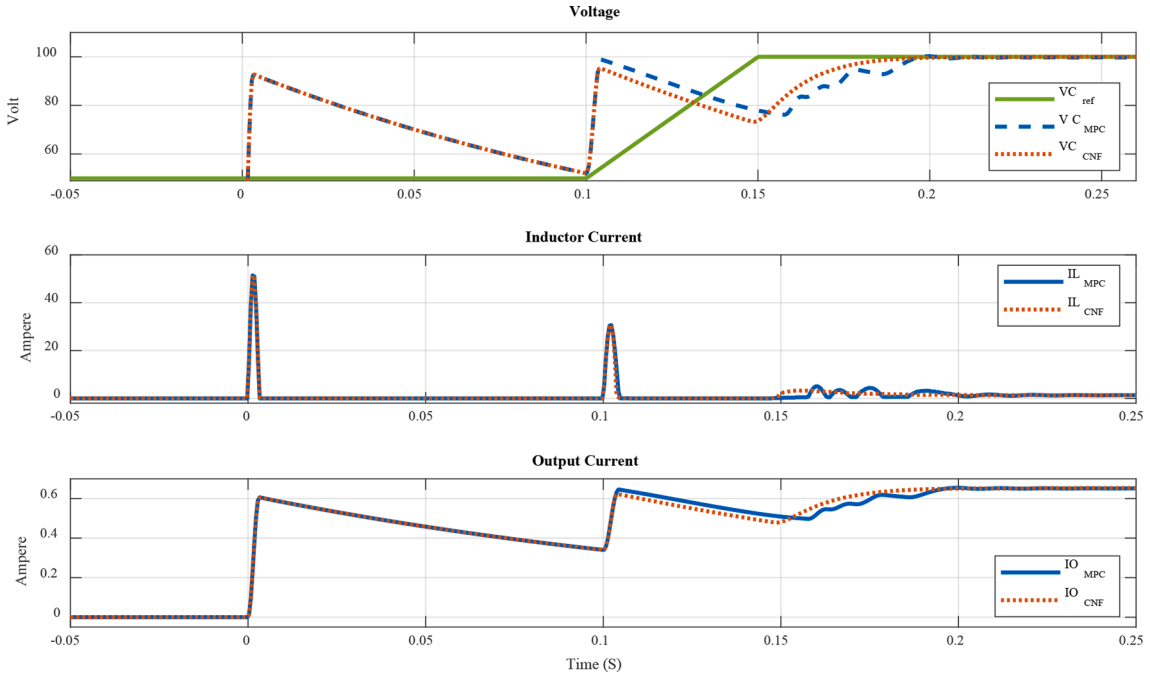

Fig. 3. Output quantities of boost converter in initial moment.

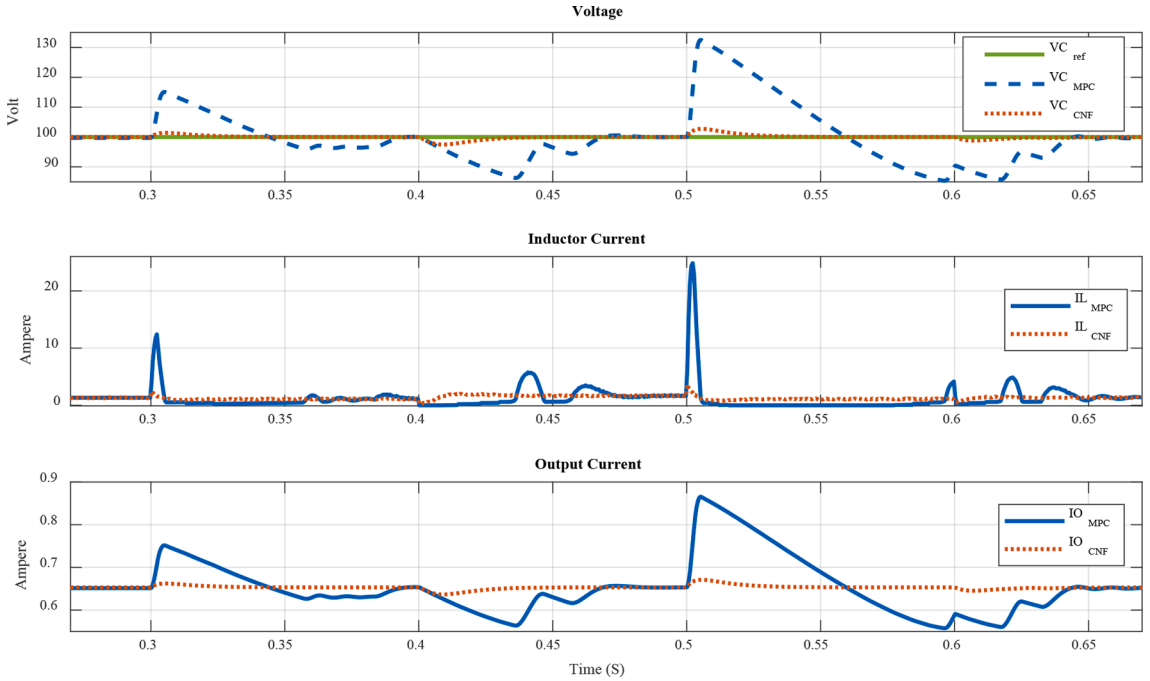

Fig. 4. Output quantities of boost converter in case of input voltage variation.

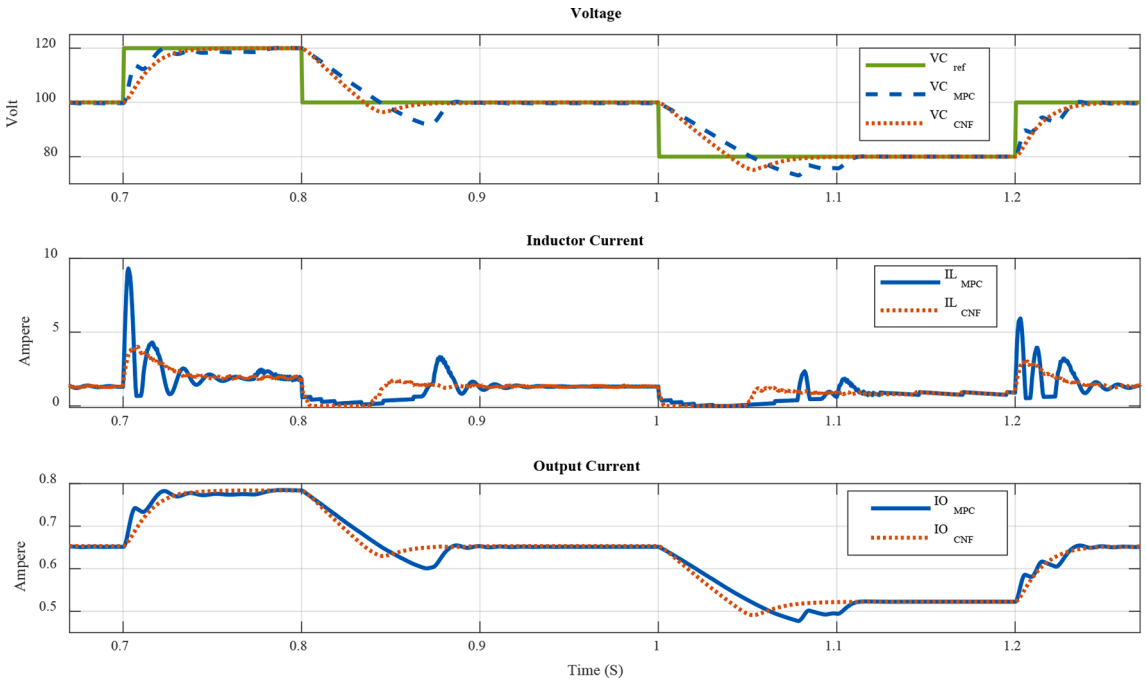

Fig. 5. Output quantities of boost converter in case of Voltage reference variation.

scenario is used to examine the proposed controller's functionality when the voltage reference is abruptly changed. To accomplish this, the voltage reference is varied from 100 to 120 to 100 to 80 to 100 V in 0.7, 0.8, and 1 s, respectively. In this case, the nonlinear controller outperforms the linear controller, resulting in the faster results shown in Fig. 5. In comparison to the linear controller, the inductance current transition is smoother and exhibits less overshoot. Eventually, the nonlinear control strategy attempts to remove the output disturbance in the presence of a load shift. The initial load resistance of 157 Ω is connected in the output circuit of the boost converter (R2 in Fig. 1). A 40Ω resistor (R1 in Fig. 1) is connected to the converter's output at $t = 1.3$ sec. Fig. 6 depicts the transitory outcomes of this event. In comparison to a linear controller, the suggested controller demonstrates no oscillation and has a smooth response.

For the CNF controller, the inductor current changes smoothly to 6 A. While in the MPC controller the inductor current is closely increased to

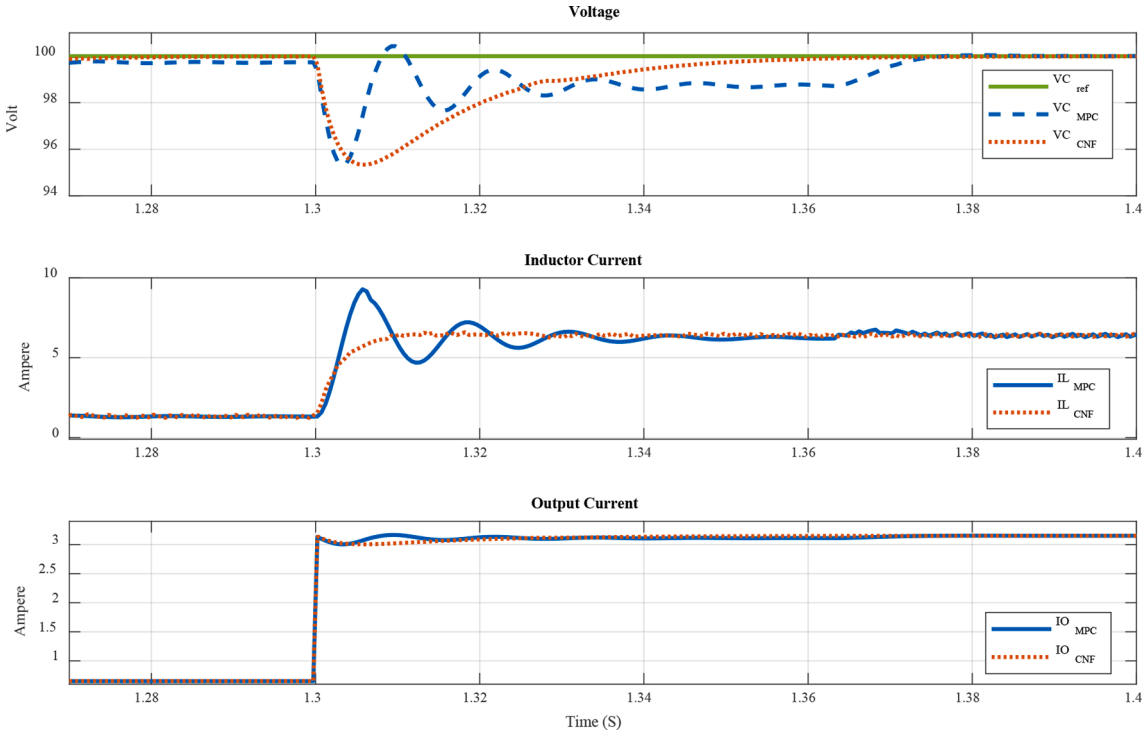

Fig. 6. Output quantities of boost converter in case of Load shift.

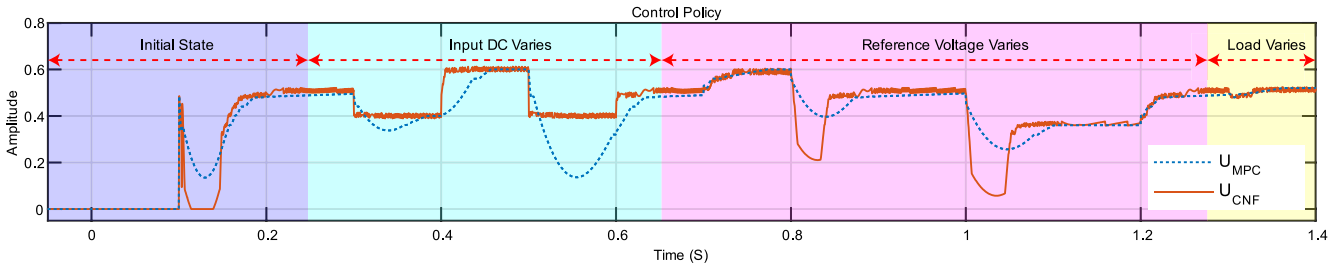

Fig. 7. Modulation index of simulation.

10 A and subsequently reduced to 6 A with fluctuation. Fig. 7 illustrates the converter's modulation index having been generated by simulation. As shown in this figure, the suggested nonlinear part of the controller has a substantial effect on modulation index at each transition.

For the sake of further improvement, a simulation scenario with different converter parameters is added to show its powerfulness under different uncertainties and parameters. Inductor and capacitor are changed to $0.645mH$ and $0.825mF$, respectively. To design the linear controller robustly, the minimum and maximum values of uncertainties are $\pm 25\%$ of the nominal values of each parameter. As can be seen from Fig. 8 the optimal controller designed by CNF has a significant improvement compared to the MPC controller. Several scenarios of input voltage change and reference change are considered. The CNF controller has a much lower overshot and settling time in comparison with the MPC controller.

5. Experimental results

Experiments are conducted to validate the suggested controller for DC/DC boost converters with variable input voltages and changing loads. As shown in Fig. 9, the dSpace MicroLabBox DS1202 is configured in a hardware-driven interrupt function that samples the measurements and computes the duty cycle of the boost converter(s) IGBT in accordance with the suggested control strategy.

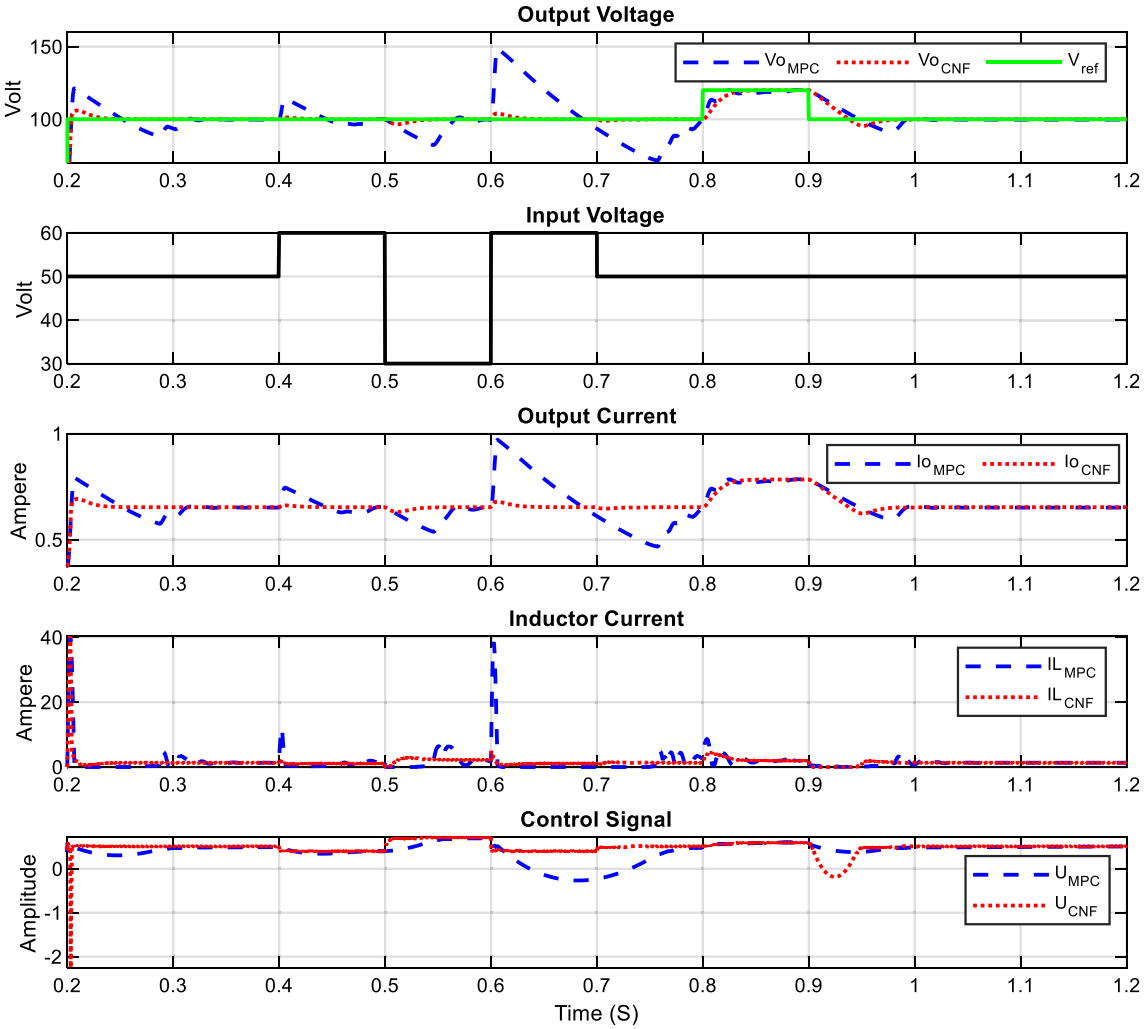

Fig. 8. Quantities of the converter under different scenarios for different inductor and capacitor values.

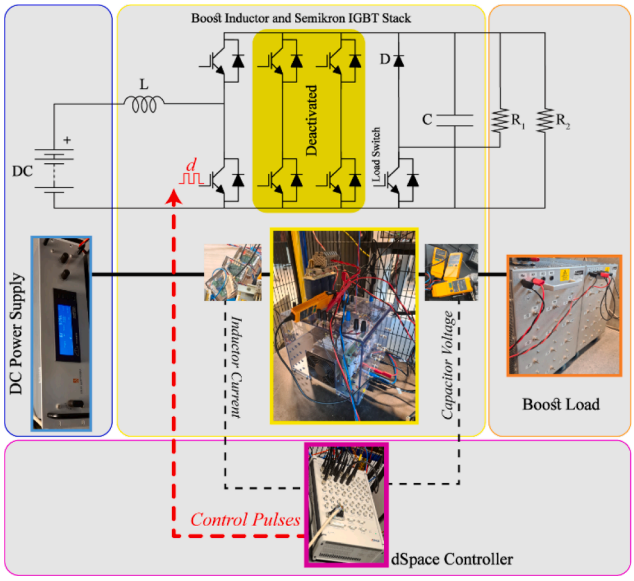

Fig. 9. The experimental setup.

As can be seen in Fig. 9, the experimental testbed employs a three-leg-6 IGBT SEMITEACH B6U + E1CIF + B6CI configuration. The bottom IGBT in leg 1 acts as an active switch in boost topology, while the IGBT in the last leg acts as a switch for the addition of the load. Additionally, the included DC link capacitors served as a voltage filter at the boost output stage. The input boost inductor is inserted between the DC Power Supply, a Delta Elektronika SM15k, and the boost IGBT switch in the first leg of the SEMITEACH stack, serving as a controlled input voltage source. The boost converter is loaded with two resistor (R1 and R2) banks of 153Ω and 40Ω, the latter of which is linked to the circuit through a programmable IGBT for ease of experiment automation.

Fig. 10 illustrates the converter's initial state quantities for both controllers when the converter begins operation. In the scope of the practical figures, the input voltage is offset by 50 V for clarity. The whole procedure of the practical examination is the same as simulation.

As can be observed, the suggested controller's output voltage converges to the setpoint more quickly. The nonlinear controller, on the other hand, increases the ripple of the inductor current because of the oscillation in modulation index generated by the CNF controller. Fig. 11 demonstrates the modulation index having been obtained by the experimental test. The CNF controller has many variations compared to the MPC one because of nonlinearity. The converter's quantities are shown in Fig. 12 in the case of DC input fluctuation. The nonlinear controller has much improved transient performance in terms of output

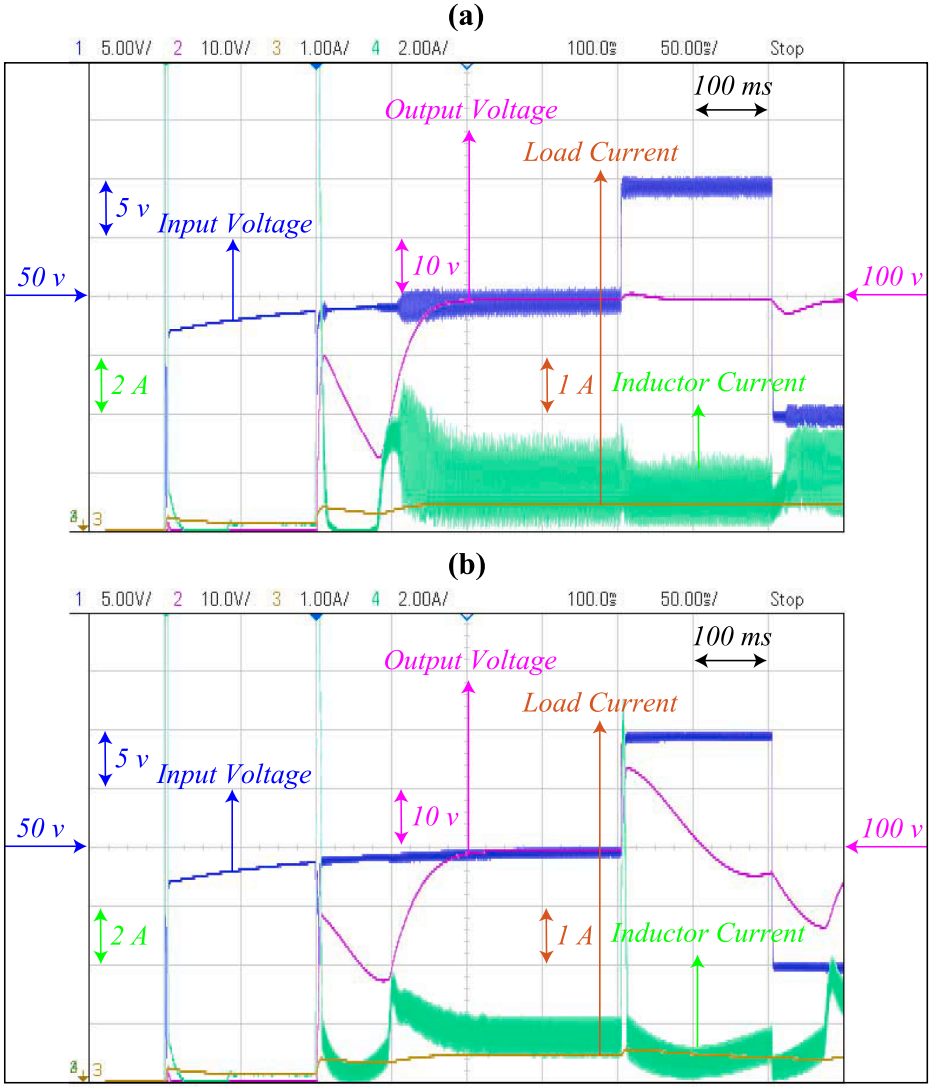

Fig. 10. Initial state of the converter quantities a) CNF controller b) MPC controller.

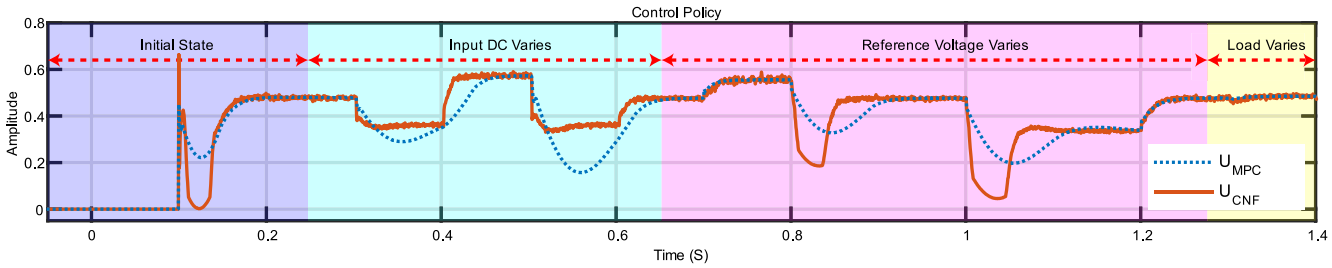

Fig. 11. Modulation index of the experiment.

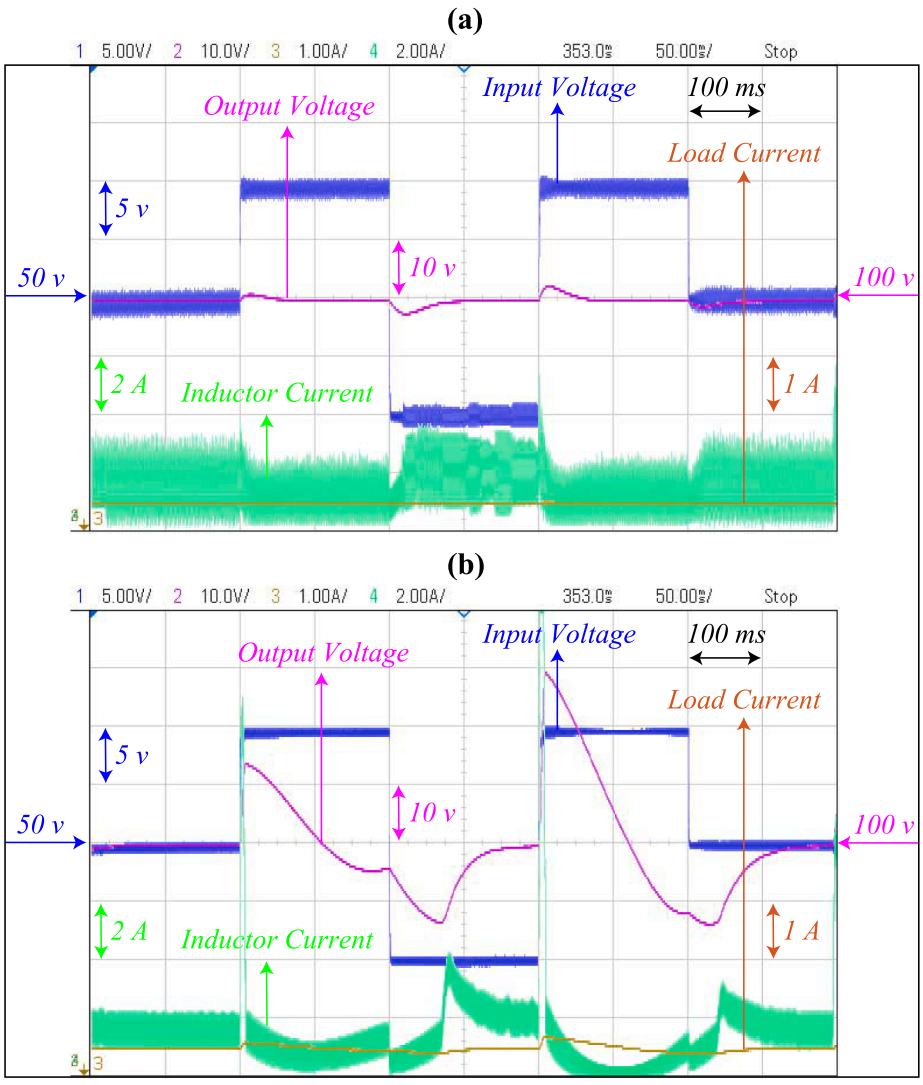

Fig. 12. Quantities of the converter under Input Voltage variation a) CNF controller b) MPC controller.

voltage, inductor current, and output current. For instance, the output voltage overshoot is reduced from 14% to less than 1% when input voltage has a sudden alteration from 50V to 60 V. Furthermore, the settling time exceeds 200ms in the case of only using linear controller; however, it significantly decreased 50ms when the CNF applied. The converter quantities are shown in fig. 13 where the voltage reference change and the load shift have been considered. The red point given in the Fig. 13 is the instant when the reference changes from 100V to 120V. Then, it decreases to 100V at the blue dot. After that, the green point is where the reference voltage declines to 80V. Finally, the orange point is the instant in which the set point comes back to 100V once again. In both cases the proposed controller completely outperforms. In terms of maximum overshoot, it should be noted that it is around 5V in the proposed strategy, which is well below the existing method. The Fig. 13 reveals that the settling times for suggested scheme are closely less than 100ms compared to the existing approach which is well over 100ms.

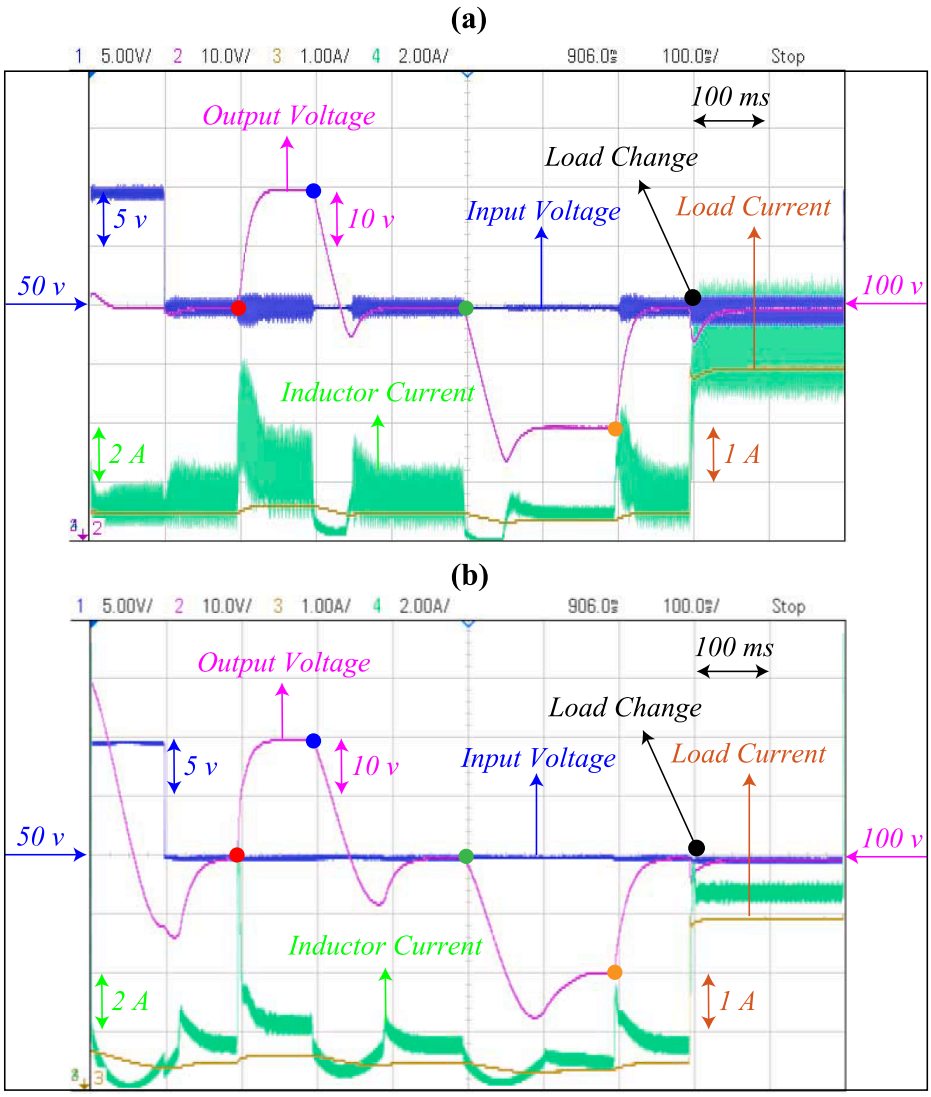

Fig. 13. Quantities of the converter under reference voltage variation and load shift a) CNF controller b) MPC controller.

6. Conclusion

DC/DC boost converters are important components of DC microgrids. As a consequence, their optimum performance under unpredictable conditions is of high priority. This article presented a new CNF control method for DC/DC boost converters. The nonlinear component is responsible for reducing the system's output overshoot based on the assigned control parameters. Its performance is highly reliant on the factors that govern it. As a result, a novel tuning technique was provided for determining the optimum parameter values. Numerous simulations and practical testing were conducted to determine the efficacy of the suggested nonlinear controller. To carry out comprehensive research, the controller with just linear components and the controller with both linear and nonlinear components were examined for testing. Various load shifts, input voltage fluctuation, and reference voltage change situations are investigated. The outcomes indicate that the suggested approach outperforms the linear controller.

CRediT authorship contribution statement

Ali Vazani: Conceptualization, Methodology, Software, Validation, Formal analysis, Writing – original draft. **Hamid Mirshekali:** Conceptualization, Methodology, Validation, Data curation, Writing – original draft, Formal analysis. **Nenad Mijatovic:** Validation, Investigation, Supervision, Writing – review & editing. **Valiollah Ghaffari:** Conceptualization, Methodology, Validation, Supervision, Writing – review & editing. **Rahman Dashti:** Conceptualization, Methodology, Software, Validation, Supervision, Writing – review & editing. **Hamid Reza Shaker:** Supervision, Writing – review & editing, Project administration. **Mohammad Mehdi Mardani:** Validation, Writing – review & editing. **Tomislav Dragičević:** Supervision, Validation, Writing – review & editing.

Declaration of Competing Interest

The authors declare that they have no known competing financial interests or personal relationships that could have appeared to influence the work reported in this paper.

Data availability

Data will be made available on request.

References

[1] Iqbal A, Bhaskar MS, Meraj M, Padmanaban S, Rahman S. Closed-Loop Control and Boundary for CCM and DCM of Nonisolated Inverting N× Multilevel Boost Converter for High-Voltage Step-Up Applications. IEEE Trans Ind Electron 2020;67:2863–74. https://doi.org/10.1109/TIE.2019.2912797.

[2] H. Mirshekali, R. Dashti, H.R. Shaker, R. Samsami, A New Model Predictive Control Based Method for Control of Grid Connected Inverter Using Predictive Functional Control, in: 2020 8th International Conference on Smart Energy Grid Engineering, SEGE 2020, Institute of Electrical and Electronics Engineers Inc., 2020: pp. 22–26. Doi: 10.1109/SEGE49949.2020.9181896.
[3] Sartipizadeh H, Harirchi F, Babakmehr M, Dehghanian P. Robust Model Predictive Control of DC-DC Floating Interleaved Boost Converter with Multiple Uncertainties. IEEE Trans Energy Convers 2021;36:1403–12. https://doi.org/10.1109/TEC.2021.3058524.
[4] Kim SK, Park CR, Kim JS, Lee YI. A stabilizing model predictive controller for voltage regulation of a DC/DC boost converter. IEEE Trans Control Syst Technol 2014;22:2016–23. https://doi.org/10.1109/TCST.2013.2296508.
[5] C. Yfoulis, An MPC Reference Governor Approach for Enhancing the Performance of Precompensated Boost DC–DC Converters, Energies 2019, Vol. 12, Page 563. 12 (2019) 563. Doi: 10.3390/EN12030563.
[6] Chincholkar SH, Jiang W, Chan CY. A Modified Hysteresis-Modulation-Based Sliding Mode Control for Improved Performance in Hybrid DC-DC Boost Converter. IEEE Trans Circuits Syst Express Briefs 2018;65:1683–7. https://doi.org/10.1109/TCSII.2017.2784549.
[7] Chen HC, Lu CY, Lien WH, Chen TH. Active Capacitor Voltage Balancing Control for Three-Level Flying Capacitor Boost Converter Based on Average-Behavior Circuit Model. IEEE Trans Ind Appl 2019;55:1628–38. https://doi.org/10.1109/TIA.2018.2876031.
[8] Kobaku T, Jeyasenthil R, Sahoo S, Ramchand R, Dragicevic T. Quantitative Feedback Design-Based Robust PID Control of Voltage Mode Controlled DC-DC Boost Converter. IEEE Trans Circuits Syst Express Briefs 2021;68:286–90. https://doi.org/10.1109/TCSII.2020.2988319.
[9] Kim SK, Ahn CK. Nonlinear Tracking Controller for DC/DC Boost Converter Voltage Control Applications via Energy-Shaping and Invariant Dynamic Surface Approach. IEEE Trans Circuits Syst Express Briefs 2019;66:1855–9. https://doi.org/10.1109/TCSII.2018.2890440.
[10] Sferlazza A, Albea-Sanchez C, Martinez-Salamero L, Garcia G, Alonso C. Min-type control strategy of a DC-DC synchronous boost converter. IEEE Trans Ind Electron 2020;67:3167–79. https://doi.org/10.1109/TIE.2019.2908597.
[11] Huangfu Y, Li Q, Xu L, Ma R, Gao F. Extended State Observer Based Flatness Control for Fuel Cell Output Series Interleaved Boost Converter. IEEE Trans Ind Appl 2019;55:6427–37. https://doi.org/10.1109/TIA.2019.2936331.
[12] Chen HC, Lu CY, Rout US. Decoupled master-slave current balancing control for three-phase interleaved boost converters. IEEE Trans Power Electron 2018;33:3683–7. https://doi.org/10.1109/TPEL.2017.2760887.
[13] Huangfu Y, Zhuo S, Chen F, Pang S, Zhao D, Gao F. Robust Voltage Control of Floating Interleaved Boost Converter for Fuel Cell Systems. IEEE Trans Ind Appl 2018;54:665–74. https://doi.org/10.1109/TIA.2017.2752686.
[14] Errouissi R, Al-Durra A, Muyeen SM. A Robust Continuous-Time MPC of a DC-DC Boost Converter Interfaced with a Grid-Connected Photovoltaic System. IEEE J Photovolt 2016;6:1619–29. https://doi.org/10.1109/JPHOTOV.2016.2598271.
[15] Oettmeier FM, Neely J, Pekarek S, DeCarlo R, Uthaichana K. MPC of switching in a boost converter using a hybrid state model with a sliding mode observer. IEEE Trans Ind Electron 2009;56:3453–66. https://doi.org/10.1109/TIE.2008.2006951.
[16] Danyali S, Hosseini SH, Gharehpetian GB. New extendable single-stage multi-input DC-DC/AC boost converter. IEEE Trans Power Electron 2014;29:775–88. https://doi.org/10.1109/TPEL.2013.2256468.
[17] Karamanakos P, Geyer T, Manias S. Direct voltage control of DC-DC boost converters using enumeration-based model predictive control. IEEE Trans Power Electron 2014;29:968–78. https://doi.org/10.1109/TPEL.2013.2256370.
[18] Mungporn P, Thounthong P, Yodwong B, Ekkaravarodome C, Bilsalam A, Pierfederici S, et al. Modeling and Control of Multiphase Interleaved Fuel-Cell Boost Converter Based on Hamiltonian Control Theory for Transportation Applications. IEEE Trans Transp Electrif 2020;6:519–29. https://doi.org/10.1109/TTE.2020.2980193.
[19] Neacsu DO, Sirbu A. Design of a LQR-Based boost converter controller for energy savings. IEEE Trans Ind Electron 2020;67:5379–88. https://doi.org/10.1109/TIE.2019.2934062.
[20] Agrawal N, Samanta S, Ghosh S. Modified LQR Technique for Fuel-Cell-Integrated Boost Converter. IEEE Trans Ind Electron 2021;68:5887–96. https://doi.org/10.1109/TIE.2020.3000096.
[21] Olalla C, Leyva R, El Aroudi A, Queinnec I. Robust LQR control for PWM converters: An LMI approach. IEEE Trans Ind Electron 2009;56:2548–58. https://doi.org/10.1109/TIE.2009.2017556.
[22] Al-Mothafar MRD, Radaideh SM, Abdullah MA. LQR-based control of parallel-connected boost dc-dc converters: A comparison with classical current-mode control. Int J Comput Appl Technol 2012;45:15–27. https://doi.org/10.1504/IJCAT.2012.050129.
[23] Habib M, Khoucha F, Harrag A. GA-based robust LQR controller for interleaved boost DC–DC converter improving fuel cell voltage regulation. Electr Pow Syst Res 2017;152:438–56. https://doi.org/10.1016/J.EPSR.2017.08.004.
[24] A. vazani, V. Ghaffari, An innovative algorithm for tuning of composite nonlinear feedback control in continuoustime systems, Asian J Control. An innovat (2022) 1–10. Doi: https:// doi.org/10.1002/asjc.2921.
[25] Xu Q, Zhang C, Wen C, Wang P. A Novel Composite Nonlinear Controller for Stabilization of Constant Power Load in DC Microgrid. IEEE Trans Smart Grid 2019;10:752–61. https://doi.org/10.1109/TSG.2017.2751755.
[26] Lin P, Zhang C, Wang J, Jin C, Wang P. On Autonomous Large-Signal Stabilization for Islanded Multibus DC Microgrids: A Uniform Nonsmooth Control Scheme. IEEE Trans Ind Electron 2020;67:4600–12. https://doi.org/10.1109/TIE.2019.2931281.
[27] Zhang M, Xu Q, Zhang C, Nordstrom L, Blaabjerg F. Decentralized Coordination and Stabilization of Hybrid Energy Storage Systems in DC Microgrids. IEEE Trans Smart Grid 2022;13:1751–61. https://doi.org/10.1109/TSG.2022.3143111.
[28] J. Lazar, S. Cuk, Open loop control of a unity power factor, discontinuous conduction mode boost rectifier, INTELEC, International Telecommunications Energy Conference (Proceedings). (1995) 671–677. Doi: 10.1109/INTLEC.1995.499030.
[29] Reatti A, Balzani M. PWM switch model of a buck-boost converter operated under discontinuous conduction mode. Midwest Symposium on Circuits and Systems 2005;2005:667–70. https://doi.org/10.1109/MWSCAS.2005.1594189.
[30] [PDF] Symbolic Analysis of PWM DC-DC Converters operated under both Continuous and Discontinuous Conduction Modes by Francesco Grasso, Antonio Luchetta, Alberto Reatti, Leonardo Serri · 2755212042 · OA.mg, (n.d.). https://oa.mg/work/2755212042 (accessed May 31, 2023).
[31] Anwar U, Maksimović D, Afridi KK. Generalized hybrid feedforward control of pulse width modulated switching converters, 2016 IEEE 17th Workshop on Control and Modeling for Power Electronics. COMPEL 2016;2016. https://doi.org/10.1109/COMPEL.2016.7556757.
[32] Unitrode, Switching Regulated Power Supply Design Seminar Manual, Unitrode Corporation, 1986.
[33] Lan W, Thum CK, Chen BM. A hard-disk-drive servo system design using composite nonlinear-feedback control with optimal nonlinear gain tuning methods. IEEE Trans Ind Electron 2010;57:1735–45. https://doi.org/10.1109/TIE.2009.2032205.
[34] Ehsani M, Saeidi M, Radmanesh H, Abrishamifar A. Comparisons between Generalized Predictive Control and Linear Controllers in Multi-Input DC-DC Boost Converter. Int J Ind Electron Control Optimiz 2020;3:27–34. https://doi.org/10.22111/IECO.2019.28584.1135.
[35] Karami Z, Shafiee Q, Khayat Y, Yaribeygi M, Dragicevic T, Bevrani H. Decentralized Model Predictive Control of DC Microgrids with Constant Power Load. IEEE J Emerg Sel Top Power Electron 2021;9:451–60. https://doi.org/10.1109/JESTPE.2019.2957231.